

# $\eta$ -superconductivity in the Hubbard chain with pair hopping

G.I. Japaridze <sup>a,b</sup>, A.P. Kampf <sup>a</sup>, M. Sekania <sup>a,c</sup>, P. Kakashvili <sup>c</sup>, and Ph. Brune <sup>a</sup>

<sup>a</sup> Institut für Physik, Theoretische Physik III, Elektronische Korrelationen und Magnetismus, Universität Augsburg, 86135 Augsburg, Germany

<sup>b</sup> Institute of Physics, Georgian Academy of Sciences, Guramishvili Str. 6, 380077, Tbilisi, Georgia

<sup>c</sup> Department of Physics, Tbilisi State University, Chavchavadze Ave. 3, 380028, Tbilisi, Georgia

The ground state phase diagram of the 1D Hubbard chain with pair-hopping interaction is studied. The analysis of the model is performed using the continuum-limit field theory approach and exact diagonalization studies. At half-filling the phase diagram is shown to consist of two superconducting states with Cooper pair center-of-mass momentum  $Q = 0$  (BCS- $\eta_0$  phase) and  $Q = \pi$  ( $\eta_\pi$ -phase) and four insulating phases corresponding to the Mott antiferromagnet, the Peierls dimerized phase, the charge-density-wave (CDW) insulator as well as an unconventional insulating phase characterized by the coexistence of a CDW and a bond-located staggered magnetization. Away from half-filling the phase diagram consists of the superconducting BCS- $\eta_0$  and  $\eta_\pi$  phases and the metallic Luttinger-liquid phase. The BCS- $\eta_0$  phase exhibits smooth crossover from a weak-coupling BCS type to a strong coupling local-pair regime. The  $\eta_\pi$  phase shows properties of the doublon (zero size Cooper pair) superconductor with Cooper pair center-of-mass momentum  $Q = \pi$ . The transition into the  $\eta_\pi$ -paired state corresponds to an abrupt change in the groundstate structure. After the transition the conduction band is completely destroyed and a new  $\eta_\pi$ -pair band corresponding to the strongly correlated doublon motion is created.

PACS numbers: 71.10.Fd, 71.10.Hf, 71.27.+a, 71.30.+h, 74.20.-z

## I. INTRODUCTION

The problem of a crossover from a weak-coupling BCS picture of Cooper pair formation [1] to a Bose-Einstein (BE) condensation of preformed local pairs has drawn special interest during the last two decades (see for a review Refs. [2,3]). Increased renewed interest to this problem mainly comes from experimental observations regarding the unusual properties of high- $T_c$  materials. Particularly important in this respect is the extreme short (of the order of one lattice spacing) coherence length of the pairs in the superconducting state [4] and a pseudo-gap structure in the normal-state density of states of underdoped cuprates [5].

Leggett [6] was the first to point out that BCS superconductivity can be continuously connected to BE condensation by increasing the two-particle attraction between electrons from weak to strong coupling. The size of Cooper pairs shrinks continuously until spatially well separated bosons form, which undergo Bose condensation at a sufficiently low temperature. Nozieres and Schmitt-Rink [7] have extended Leggett's work to lattice electrons and analyzed the crossover between the BCS and the BE limit as a function of coupling strength. The attractive ( $U < 0$ ) Hubbard model

$$\mathcal{H} = -t \sum_{n,\sigma} (c_{n,\sigma}^\dagger c_{n+1,\sigma} + h.c.) + U \sum_n \hat{\rho}_\uparrow(n) \hat{\rho}_\downarrow(n) \quad (1)$$

was usually considered to describe the evolution from the BCS type pairing to the local pair (composite boson) limit [8–17]. Here  $c_{n,\sigma}^\dagger$  ( $c_{n,\sigma}$ ) is the creation (annihilation) operator for an electron with spin  $\sigma$  at site  $n$  and  $\hat{\rho}_\sigma(n) = c_{n,\sigma}^\dagger c_{n,\sigma}$ .

A rather different realization of local-pairing is the  $\eta$ -pairing mechanism of superconductivity introduced by Yang [18]. Yang discovered a class of eigenstates of the Hubbard Hamiltonian which have the property of off-diagonal long-range order (ODLRO) [19], which in turn implies the Meissner effect and flux quantization [20,21]. These eigenstates are constructed in terms of doublon (on-site singlet pair) creation operators and can be shown to be of very high energy compared to the global ground state [18]. Following Yang's notations we call these  $\eta$ -paired states. On a bipartite lattice one can consider two different realizations of the  $\eta$ -paired state, constructed in terms of zero size Cooper pairs with *center-of-mass momentum* equal to zero ( $\eta_0$ -pairing) and  $\pi$  ( $\eta_\pi$ -pairing), respectively. Yang also proved that these states cannot be ground states for the Hubbard model with finite interaction [18]. The  $\eta_0$ -superconductivity is realized in the Hubbard model only at infinite on-site attraction [22]. Shortly after Yang's paper, Eßler, Korepin, and Schoutens proposed the supersymmetric extension of the Hubbard model showing a true ODLRO and  $\eta_0$ -superconductivity in the ground state for a finite on-site interaction [23]. Later on several other integrable generalizations of the Hubbard model, with  $\eta_0$  type ordering in the ground state were proposed [24]. The important common feature for all integrable models of  $\eta$ -superconductivity is the high  $SU(2) \otimes SU(2)$  symmetry which is ensured by the *strongly correlated kinematics* of electrons on a lattice.

Another model with a *kinematical mechanism* for the formation of Cooper pairs is the Penson-Kolb (PK) model [25]. The Hamiltonian of the PK model contains, in addition to the usual one-electron hopping term, a

term that moves singlet pairs of electrons from site to site and in the one-dimensional case is given by

$$\begin{aligned}\mathcal{H} = & -t \sum_{n,\alpha} (c_{n,\alpha}^\dagger c_{n+1,\alpha} + h.c.) \\ & + W \sum_n (\hat{q}_\uparrow(n) \hat{q}_\downarrow(n) + h.c.).\end{aligned}\quad (2)$$

where  $\hat{q}_\sigma(n) = c_{n,\sigma}^\dagger c_{n+1,\sigma}$ . In the case  $W < 0$  the PK model (2) describes a continuous evolution of the usual BCS type superconducting state at  $|W| \ll t$  into a local pair  $\eta_0$ -type state at  $|W| \gg t$  [26]. More important is that in the case of “repulsive” pair-hopping interaction ( $W > 0$ ), the  $\eta_\pi$ -paired state is realized in the ground state of the PK model for  $W > W_c \simeq 2t$  [27–29].

It is notable that the pair-hopping term and the Hubbard term could be obtained from the same general tight-binding Hamiltonian [30] by focusing on selected terms of the two-particle interaction. Indeed the same matrix element of the electron-electron interaction potential  $V(r)$ ,  $V(n, m, k, l) = \langle n, m | V(r) | k, l \rangle$  which gives rise to the on-site Hubbard interaction for  $n = m = k = l$  leads to the pair-hopping amplitude  $W$  for  $n = m$  and  $k = l = n \pm 1$ . Although originating from the same two-body potential the Hubbard and the pair-hopping couplings represent different types of correlations in the electron system. If the Hubbard term describes on-site correlations, the site-off-diagonal pair-hopping term describes part of the so-called “bond-charge” interaction. The sign of *Coulomb-driven* on-site and pair-hopping interaction is typically repulsive  $U, W > 0$ . However, we will treat the parameters  $U, W$  as the effective ones, assuming that they include all the possible renormalizations. In particular, contribution from the strong electron-phonon coupling or from the coupling between electrons and other electronic subsystem could give the effective attractive on-site ( $U < 0$ ) interaction [2]. The “attractive” ( $W < 0$ ) pair-hopping term can originate from the coupling of electrons with intermolecular vibrations [31], or from the on-site hybridization term in a generalized periodic Anderson model [32].

In this paper we investigate the interplay between these different sources for local pair formation: the site-diagonal Hubbard attraction and the site-off-diagonal pair-hopping interaction. We consider the extended Hubbard chain with pair-hopping interaction i.e. the so-called Penson-Kolb-Hubbard (PKH) model [33]. In one-dimension the Hamiltonian reads:

$$\begin{aligned}\mathcal{H} = & -t \sum_{n,\sigma} (c_{n,\sigma}^\dagger c_{n+1,\sigma} + h.c.) + U \sum_n \hat{\rho}_\uparrow(n) \hat{\rho}_\downarrow(n) \\ & + W \sum_n (\hat{q}_\uparrow(n) \hat{q}_\downarrow(n) + h.c.) + \mu \sum_{n,\sigma} \hat{\rho}_\sigma(n).\end{aligned}\quad (3)$$

There are  $N_e$  particles,  $N_0$  sites and the band filling  $\nu = N_e/2N_0$  is controlled by the chemical potential  $\mu$ . In the absence of the  $W$  term the Hamiltonian (3) corresponds

to the Hubbard model, while in the absence of the  $U$  term it reduces to the Penson-Kolb model.

The PKH model has been investigated mainly in the case  $U > 0$  [33,28,34–36]. Recently Robaszkiewicz and Bułka studied the  $U < 0$  PKH model by means of the Hartree-Fock approximation and the slave-boson mean-field method [37]. In this paper we focus on the nature of phase transitions in the ground state of the PKH model between the following local-pair ordered phases in [37,36]: the  $\eta_0$ -superconductor, the CDW phase, and the  $\eta_\pi$ -superconductor.

The paper is organized as follows: In Sect. II we review the model and its symmetries. We study the ground state phase diagram of the PKH chain using the continuum-limit bosonization approach (Sect III) and exact Lanczos diagonalization for chains up to  $L = 12$  sites (Sect. IV). Finally, Sect. V is devoted to a discussion and to concluding remarks.

## II. REVIEW OF THE PKH MODEL

There are two important aspects distinguishing the PKH model from the Hubbard model: the symmetry of these models and the nonlocal character of the pair-hopping interaction.

Let us first consider the *symmetry* aspect. The PKH model and the Hubbard model are characterized by the same  $SU(2)$ -spin symmetry. The difference lies in the symmetry of the corresponding charge sectors -  $SU(2)$  in the case of the 1/2-filled Hubbard model and  $U(1)$  in the case of the PK model. This can be easily seen for a strong Hubbard attraction  $|U| \gg |W|, t$  where a large gap of order  $|U|$  exists in the single-particle excitation spectrum. Projecting the system on the subspace excluding single occupancy of sites and using the standard second-order perturbation theory with respect to  $t^2/|U|$  [38] one obtains the following effective spin-1/2  $XXZ$  spin chain Hamiltonian

$$\begin{aligned}\mathcal{H} = & E_0 + J \sum_n \left[ \frac{1}{2} (\eta_0^+(n) \eta_0^-(n+1) + h.c.) \right. \\ & \left. + \Delta \eta_0^z(n) \eta_0^z(n+1) \right],\end{aligned}\quad (4)$$

where  $E_0 = -\frac{1}{2} N_0 |U|$ ,

$$J = 2W - \frac{4t^2}{|U|}, \quad \Delta = \frac{4t^2/|U|}{|2W - 4t^2/|U||} \quad (5)$$

and the pseudospin operators are

$$\begin{aligned}\eta_0^+(n) &= c_{n,\uparrow}^\dagger c_{n,\downarrow}^\dagger, \quad \eta_0^-(n) = c_{n,\downarrow} c_{n,\uparrow}, \\ \eta_0^z(n) &= (c_{n,\uparrow}^\dagger c_{n,\uparrow} + c_{n,\downarrow}^\dagger c_{n,\downarrow} - 1)/2.\end{aligned}\quad (6)$$

As we see the charge sectors of the half-filled PKH and Hubbard models are governed by the  $U(1)$  ( $\Delta \neq 1$ )

and the  $SU(2)$  ( $\Delta = 1$ ) symmetry of the equivalent Heisenberg model respectively. In the case of the half-filled Hubbard model, due to the  $SU(2)$ -charge symmetry, the superconducting order mixes with the charge density order. The singlet superconducting (SS) and the charge density wave (CDW) correlations show an identical power-law decay in the infrared (large distance) limit [39].

For  $W \neq 0$  ( $\Delta \neq 1$ ) the spin  $\eta = 1/2$  antiferromagnet, with Hamiltonian (4) is in a *gapless planar XY* phase for  $\Delta \leq 1$  and in the *gapped Néel phase* for  $\Delta > 1$  [40]. The Néel phase is realized for  $0 < W < 4t^2/|U|$  and corresponds to the insulating long-range-ordered (LRO) CDW state in terms of the initial electron system. The gapless planar *XY* phase is realized for  $W < 0$  and  $W > 4t^2/|U|$ . The tendency towards in-plane magnetic ordering reflects to the superconducting ordering within the initial electron system.

In the ultimate limit  $t^2/|U| \rightarrow 0$  the PKH model is equivalent to the spin-1/2 *XY* model. Electrons only appear in singlet pairs on the same site, the interaction simply acts as a hopping term for these pairs. The model is  $\eta$ -superconducting by construction. The CDW correlations

$$\langle \eta_0^z(0)\eta_0^z(n) \rangle \simeq (-1)^n \cdot n^{-2} \quad (7)$$

decay faster than the  $\eta$ -superconducting correlations

$$\langle \eta_0^+(0)\eta_0^-(n) \rangle \simeq n^{-1/2}. \quad (8)$$

This picture holds true for arbitrary  $W$ . However, if the  $\eta_0$ -ordering is realized for  $W < 0$ , then in the case of a "repulsive" ( $W > 0$ ) pair-hopping coupling, the  $\eta_\pi$ -superconducting correlations

$$\langle \eta_\pi^+(0)\eta_\pi^-(n) \rangle \simeq (-1)^n \cdot n^{-1/2} \quad (9)$$

have to dominate. In deriving (9) the unitary transformation  $\eta_0^+(n) \rightarrow (-1)^n \eta_0^+(n) \equiv \eta_\pi^+(n)$  has been used which changes the sign of the transverse exchange  $J_\perp \rightarrow -J_\perp$ .

Although the *XY* model is invariant with respect to a sign change of the coupling constant,  $W \rightarrow -W$  is not a symmetry of the PKH model. Therefore the way, the system approaches its limiting behaviour at  $|W| \gg t^2/|U|$  is genuinely different for negative and positive  $W$ .

The origin of this difference arises from the *site-off-diagonal nature* of the pair-hopping term. As far as the essence of the  $W \leftrightarrow -W$  asymmetry is connected to two different possibilities for Bose condensation of Cooper pairs with momentum  $Q = 0$  and  $Q = \pi$  it is convenient to rewrite the Hamiltonian (3) in momentum space as

$$\mathcal{H} = -2t \sum_{k,\sigma} c_{k,\sigma}^\dagger c_{k,\sigma} \cos(k) + \sum_Q V(Q) A_Q^\dagger A_Q. \quad (10)$$

Here  $V(Q) = U + 2W \cos(Q)$  and

$$A_Q^\dagger = \frac{1}{\sqrt{L}} \sum_k c_{k,\uparrow}^\dagger c_{Q-k,\downarrow}^\dagger \quad (11)$$

is the creation operator for a pair of electrons with opposite spins and total momentum  $Q$ .

In the weak-coupling (large bandwidth) limit  $U, W \ll t$  only scattering processes involving states near the two Fermi points  $k_F = \pm\pi\nu$  are relevant. Therefore, the scattering processes with  $Q \sim 0$  (forward scattering without and with spin flip) are characterized by the effective coupling constant  $V_{FS}(Q \ll k_F) \simeq U + 2W$  and the umklapp scattering with  $Q \sim \pi$  by the effective amplitude coupling constant  $V_{Umk}(Q \sim \pi) \simeq U - 2W$ . The umklapp scattering is irrelevant at noncommensurate band filling  $\nu \neq 1/2$ . Therefore, at  $\nu \neq 1/2$  the weak-coupling phase diagram of the PKH model has to be similar to that of the Hubbard model with an effective interaction  $U_{eff} = U + 2W$  [34–36]. At half-filling the umklapp scattering is relevant in the case of repulsive interaction ( $U, W > 0$ ) and leads to the CDW type ordering in the PKH model at  $0 < U < 2W$  [36].

In the forthcoming section we will use the continuum-limit bosonization approach to study the ground state phase diagram of the PKH model. However, already the above presented qualitative analysis indicates the absence of the  $\eta_\pi$ -superconducting phase in the weak-coupling phase diagram.

The particularity of the model in the case of strong pair-hopping interaction ( $|W| \gg t$ ) could be observed even in the simple case of *two particles* with opposite spins on the lattice. As far as the total momentum of the system  $Q_{tot}$  is conserved, one can treat each  $Q$ -sector of the Hilbert space independently. Since the ground state belongs to the sectors with  $Q_{tot} = 0$  or  $Q_{tot} = \pi$ , we restrict ourselves to these sectors only. The states with  $Q_{tot} \neq 0$  or  $\pi$  exhibit a broken time reversal symmetry and are excited states.

Let us first consider the  $U = 0$  case. At  $W = 0$  the ground state energy is  $E_0 = -4t$  and the total momentum is  $Q_{tot} = 0$ . The probability to find the on-site pair in the ground state is  $1/L$ . Eigenstates in the  $Q_{tot} = \pi$  sector correspond to the highly excited states with the energy  $E = 0$ . At  $|W|/t \rightarrow \infty$  the  $\eta_0$  pair given by the wave function  $A_0^\dagger |0\rangle$  has the energy  $E_{\eta_0} = 2W$  while the  $\eta_\pi$  pair given by the wave function  $A_\pi^\dagger |0\rangle$  has the energy  $E_{\eta_\pi} = -2W$ . Therefore, for  $W < 0$ , the groundstate *always* remains in the  $Q_{tot} = 0$  subspace and its energy continuously varies from  $-4t$  ( $W = 0$ ) to  $-2|W|$  ( $|W| \gg t$ ). The probability to find the on-site pair increases *continuously* up to 1 ( $|W|/t \rightarrow \infty$ ). In contrast, for  $W > 0$ , the energy of an  $\eta_0$ -paired state goes to  $E_{\eta_0} = 2W > 0$  while the energy of an  $\eta_\pi$ -paired state  $E_{\eta_\pi} = -2W < 0$ . Thus, with increasing  $W/t$ , at some critical value of the pair-hopping coupling  $W_c > 0$ , the total momentum of the system in the ground state should change from  $Q_{tot} = 0$  to  $Q_{tot} = 0$ . In the  $Q_{tot} = \pi$  sector the contribution of the one-particle hopping term to the energy vanishes. Below we will refer to this phenomenon as the *collapse*

of a one-particle band. On the other hand the contribution of the delocalization energy for an  $\eta_\pi$  pair is equal to  $-2W$ . Therefore one can roughly estimate the critical value to be  $W_c \simeq -2t$ .

We now consider the effect of the Hubbard interaction. It is clear that the on-site repulsion  $U > 0$  increases the difference between the unpaired state in the  $Q_{tot} = 0$  sector and the  $\eta_\pi$ -paired state in the  $Q_{tot} = \pi$  sector. Therefore the critical value has to increase in the case of on-site repulsion. Contrary, the attractive Hubbard interaction  $U < 0$  supports the on-site pairing, reduces the effect of the  $t$ -term and therefore the difference between the lowest energy states in the  $Q_{tot} = 0$  and  $Q_{tot} = \pi$  sectors. Therefore, in agreement with the strong-coupling analysis the critical value has to strongly decrease in the case of on-site attraction. As we show below, the picture remains qualitatively similar in the case of many particle systems. The essence of the transition into an  $\eta_\pi$ -paired state consists of a collapse of the one-particle band and the creation of a strongly correlated two-particle  $\eta$ -pair band.

### III. WEAK-COUPING PHASE DIAGRAM.

The field theory treatment of 1D systems of correlated electrons is based on the weak-coupling approach ( $|U|, |W| \ll t$ ). Assuming that the low energy physics is controlled by states near the Fermi points  $\pm k_F$  ( $k_F a_0 = \pi\nu$ , where  $a_0$  is the lattice spacing) we linearize the spectrum around these points and obtain two species (for each spin projection  $\sigma$ ) of fermions,  $R_\sigma(n)$  and  $L_\sigma(n)$ , which describe excitations with dispersion relations  $E(p) = \pm v_F p$ . Here,  $v_F = 2t a_0 \sin(\pi\nu)$  is the Fermi velocity and the momentum  $p$  is measured from the two Fermi points. More explicitly, one decomposes the momentum expansion for the initial lattice operators into two parts centered around  $\pm k_F$  to obtain the mapping:

$$c_{n,\sigma} \rightarrow e^{i\pi\nu n} R_\sigma(n) + e^{-i\pi\nu n} L_\sigma(n), \quad (12)$$

where the fields  $R_\sigma(n)$  and  $L_\sigma(n)$  describe right and left-moving particles, respectively, and are assumed to be smooth on the scale of the lattice spacing. This allows us to introduce the continuum fields  $R_\sigma(x)$  and  $L_\sigma(x)$  by

$$\begin{aligned} R_\sigma(n) &\rightarrow \sqrt{a_0} R_\sigma(x = na_0), \\ L_\sigma(n) &\rightarrow \sqrt{a_0} L_\sigma(x = na_0). \end{aligned} \quad (13)$$

In terms of the continuum fields the free Hamiltonian reads:

$$\mathcal{H}_0 = -iv_F \sum_\sigma \int dx [ : R_\sigma^\dagger \partial_x R_\sigma : - : L_\sigma^\dagger \partial_x L_\sigma : ] \quad (14)$$

which is recognized as the Hamiltonian of a free massless Dirac field. Here and below  $:\dots:$  denotes normal ordering with respect to the ground state of the free electron system.

The advantage of the linearization of the spectrum is twofold: the initial lattice problem is reformulated in terms of smooth continuum fields and – using the bosonization procedure – is mapped to the theory of two independent (in the weak-coupling limit) quantum Bose fields describing charge and spin degrees of freedom, respectively.

In terms of the continuum fields the initial lattice operators have the form:

$$\begin{aligned} \hat{\rho}_\sigma(n) &\rightarrow a_0 \left\{ (J_{R,\sigma}(x) + J_{L,\sigma}(x)) \right. \\ &\quad \left. + (e^{-i2\pi\nu n} R_\sigma^\dagger(x) L_\sigma(x) + h.c.) \right\}, \end{aligned} \quad (15)$$

$$\begin{aligned} \hat{q}_\sigma(n) &\rightarrow a_0 \left\{ (e^{+i\pi\nu} J_{R,\sigma} + e^{-i\pi\nu} J_{L,\sigma}) \right. \\ &\quad \left. + (e^{-i\pi\nu(2n+1)} R_\sigma^\dagger(x) L_\sigma(x) + h.c.) \right\}, \end{aligned} \quad (16)$$

where

$$J_{R,\sigma} \equiv : R_\sigma^\dagger(x) R_\sigma(x) :, \quad J_{L,\sigma} \equiv : L_\sigma^\dagger(x) L_\sigma(x) :.$$

The second step is to use the standard bosonization expressions for fermionic bilinears [41]:

$$\begin{aligned} -i \sum_\sigma [ : R_\sigma^\dagger \partial_x R_\sigma : - : L_\sigma^\dagger \partial_x L_\sigma : ] &\rightarrow \\ \frac{1}{2} \{ (\partial_x \theta_c)^2 + (\partial_x \phi_c)^2 \} + \frac{1}{2} \{ (\partial_x \theta_s)^2 + (\partial_x \phi_s)^2 \}, \end{aligned} \quad (17)$$

$$J_{R,\sigma} + J_{L,\sigma} \rightarrow \frac{1}{\sqrt{2\pi}} [(\partial_x \phi_c) + \sigma(\partial_x \phi_s)], \quad (18)$$

$$J_{R,\sigma} - J_{L,\sigma} \rightarrow \frac{1}{\sqrt{2\pi}} [(\partial_x \theta_c) + \sigma(\partial_x \theta_s)] \quad (19)$$

$$R_\sigma^\dagger(x) L_\sigma(x) \rightarrow \frac{-i}{2\pi a_0} \exp(i\sqrt{2\pi}(\phi_c + \sigma\phi_s)). \quad (20)$$

We thereby obtain

$$\begin{aligned} \hat{\rho}_\sigma(n) &\rightarrow a_0 \left\{ \frac{1}{\sqrt{2\pi}} [(\partial_x \phi_c) + \sigma(\partial_x \phi_s)] \right. \\ &\quad \left. - \frac{1}{\pi a_0} \sin(\sqrt{2\pi}(\phi_c + \sigma\phi_s) - 2n\pi\nu) \right\}, \end{aligned} \quad (21)$$

$$\begin{aligned} \hat{q}_\sigma(n) &\rightarrow a_0 \left\{ \frac{1}{\sqrt{2\pi}} \cos(\pi\nu) [(\partial_x \phi_c) + \sigma(\partial_x \phi_s)] \right. \\ &\quad \left. + \frac{i}{\sqrt{2\pi}} \sin(\pi\nu) [(\partial_x \theta_c) + \sigma(\partial_x \theta_s)] \right. \\ &\quad \left. - \sin(\sqrt{2\pi}(\phi_c + \sigma\phi_s) - (2n+1)\pi\nu) \right\}, \end{aligned} \quad (22)$$

Here scalar fields  $\phi_{c,s}(x)$  describe the charge and the spin degrees of freedom and fields  $\theta_{c,s}(x)$  are their dual counterparts:  $\partial_x \theta_{c,s} = \Pi_{c,s}$  where  $\Pi_{c,s}$  is the momentum conjugate to the field  $\phi_{c,s}$ . Inserting the relations (21)-(22) into (3), by virtue of the smooth variation of the fields  $\phi_{c,s}(x)$  on the scale of lattice spacing one can convert sums into integrals  $\sum_n a_0 \rightarrow \int dx$  and take the continuum limit.

All terms in the obtained continuum-limit Hamiltonian that contain the rapidly oscillating phase factors  $e^{\pm i2n\pi\nu}$  and  $e^{\pm i4n\pi\nu}$  will drop out except at  $\nu = 1/2$ , where terms containing  $e^{\pm i4n\pi\nu} = 1$ , are not oscillating and have to be kept. Performing this procedure, after rescaling of fields and lengths, the continuum-limit version of the Hamiltonian (3) acquires the following form:

$$\mathcal{H} = \mathcal{H}_c + \mathcal{H}_s \quad (23)$$

where

$$\begin{aligned} \mathcal{H}_s = \int dx \left\{ \frac{v_s}{2} [(\partial_x \varphi_s)^2 + (\partial_x \vartheta_s)^2] \right. \\ \left. + \frac{m_s}{2\pi^2 a_0^2} \cos(\sqrt{8\pi K_s} \varphi_s(x)) \right\} \end{aligned} \quad (24)$$

describes the spin degrees of freedom.

The charge degrees of freedom for  $\nu \neq 1/2$  are described by the free scalar field

$$\mathcal{H}_c = \frac{v_c}{2} \int dx [(\partial_x \varphi_c)^2 + (\partial_x \vartheta_c)^2], \quad (25)$$

and for  $\nu = 1/2$  by the quantum sine-Gordon field

$$\begin{aligned} \mathcal{H}_c = \int dx \left\{ \frac{v_c}{2} [(\partial_x \varphi_c)^2 + (\partial_x \vartheta_c)^2] \right. \\ \left. + \frac{m_c}{2\pi^2 a_0^2} \cos(\sqrt{8\pi K_c} \varphi_c(x)) \right\}. \end{aligned} \quad (26)$$

Here we have defined

$$K_c \simeq 1 + \frac{1}{2} g_c \equiv 1 - \frac{1}{2} \frac{U + 2W}{2\pi t}, \quad (27)$$

$$m_c = -\frac{U - 2W}{2\pi t} \quad (28)$$

$$K_s \simeq 1 + \frac{1}{2} g_s \equiv 1 + \frac{1}{2} \frac{U + 2W}{2\pi t}, \quad (29)$$

$$m_s = \frac{U + 2W}{2\pi t}, \quad (30)$$

$$v_c = v_F K_c^{-1}, \quad v_s = v_F K_s^{-1}. \quad (31)$$

The mapping of the Hamiltonian (3) into the quantum theory of two independent charge and spin Bose fields, allows to study the ground state phase diagram of the initial electron system, using the far-infrared properties of the bosonic Hamiltonians (24)-(26).

### A. Renormalization group analysis

Let us first consider the half-filled band case when both the spin and the charge sectors of the system are governed by the quantum sine-Gordon (SG) fields (24) and (26). The infrared behavior of the SG Hamiltonian  $\mathcal{H}_{c,s}$  is described by the corresponding pair of renormalization group (RG) equations for the effective coupling constants  $M_{c(s)}$  and  $K_{c(s)}$  [42]

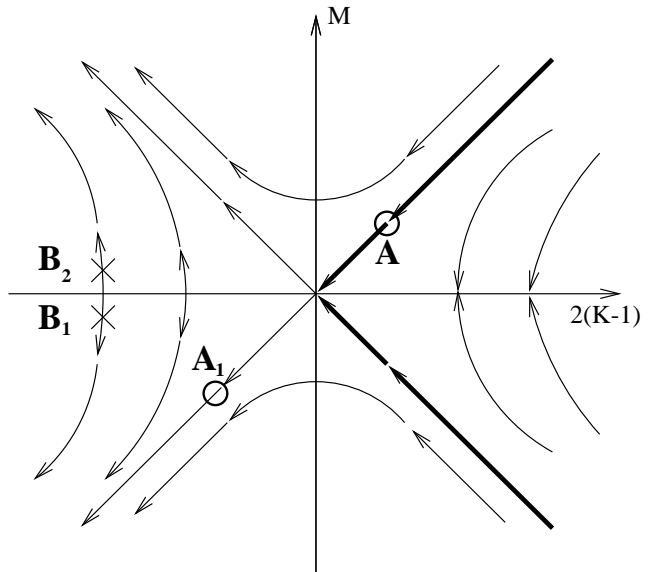


FIG. 1. Renormalization-group flow diagram; the arrows denote the direction of flow with increasing length scale. The circles correspond to the starting points in the case of a gapless (A) and a gapped ( $A_1$ ) spin channel. The crosses correspond to the starting points for two different gapped sectors in the charge channel with  $\langle \varphi_c \rangle = 0$  ( $B_1$ ) and  $\langle \varphi_c \rangle = \pi/8K_c$  ( $B_2$ ).

$$\begin{aligned} \frac{dM_{c(s)}(L)}{dL} &= -2(K_{c(s)}(L) - 1)M_{c(s)}(L) \\ \frac{dK_{c(s)}(L)}{dL} &= -\frac{1}{2}M_{c(s)}^2(L), \end{aligned} \quad (32)$$

where  $L = \ln(a_0)$ ,  $K_{c(s)}(0) = 1 + \frac{1}{2}g_{c(s)}$  and  $M_{c(s)}(0) = m_{c(s)}$ . Each pair of RG equations (32) describes the Kosterlitz-Thouless transition [43] in the charge and spin channels. The flow lines lie on the hyperbola

$$4(K_{c(s)} - 1)^2 - M_{c(s)}^2 = \mu_{c(s)}^2 = g_{c(s)}^2 - m_{c(s)}^2, \quad (33)$$

and – depending on the relation between the bare coupling constants  $g_{c(s)} \equiv 2(K_{c(s)} - 1)$  and  $m_{c(s)}$  – exhibit two different regimes (see Fig.1):

For  $g_{c(s)} \geq |m_{c(s)}|$  we are in the weak coupling regime; the effective mass  $M_{c(s)} \rightarrow 0$ . The low energy (large distance) behavior of the gapless charge (spin) excitations is described by a free scalar field. The corresponding correlations show a power law decay

$$\langle e^{i\sqrt{2\pi K^*}\varphi(x)} e^{-i\sqrt{2\pi K^*}\varphi(x')} \rangle \sim |x - x'|^{-K^*}, \quad (34)$$

$$\langle e^{i\sqrt{2\pi/K^*}\theta(x)} e^{-i\sqrt{2\pi/K^*}\theta(x')} \rangle \sim |x - x'|^{-1/K^*}, \quad (35)$$

and the only parameter controlling the infrared behavior in the gapless regime is the fixed-point value of the effective coupling constants  $K_{c(s)}^*$ .

For  $g_{c(s)} < |m_{c(s)}|$  the system scales into a strong coupling regime: depending on the sign of the bare mass

$m_{c(s)}$ , the effective mass  $M_{c(s)} \rightarrow \pm\infty$ , which signals the crossover into a strong coupling regime and indicates the dynamical generation of a commensurability gap in the excitation spectrum. The field  $\varphi_{c(s)}$  gets ordered with the vacuum expectation values [44]

$$\langle \varphi \rangle = \begin{cases} \sqrt{\frac{\pi}{8K_{c(s)}}} & (m_{c(s)} > 0) \\ 0 & (m_{c(s)} < 0) \end{cases}. \quad (36)$$

The ordering of these fields determines the symmetry properties of the possible ordered groundstates of the fermionic system.

Using Eqs. (27)-(31) and (36) one easily finds that there is a gap in the spin excitation spectrum ( $M_s \rightarrow -\infty$ ) for  $U + 2W < 0$ . In the spin-gap sector the  $\varphi_s$  field gets ordered with vacuum expectation value  $\langle \varphi_s \rangle = 0$ . In the sector  $U + 2W \geq 0$  the spin excitations are gapless ( $M_s \rightarrow 0$ ) and the low-energy properties of the spin sector are described by the free Bose field system with the fixed-point value of the parameter  $K_s^* = 1$ .

At half-filling the charge sector is gapless for  $U, W \leq 0$  and along the line  $U = 2W$  for  $U, W > 0$ . At  $U, W \leq 0$  the low-energy properties of the gapless charge sector are described by the free Bose field Hamiltonian (25) with the fixed-point value of the parameter

$$K_c^* \simeq 1 + \sqrt{2UW}/2\pi t. \quad (37)$$

For  $U, W > 0$  the line  $U = 2W$  ( $m_c = 0$ ) corresponding to the unstable fixed-point line  $m_c = 0, K_c - 1 < 0$  (see Fig. 1). Here the infrared properties of the gapless charge sector are described by the free massless Bose field with the bare value of the Luttinger liquid parameter  $K_c$ . Moreover, the line  $m_c = 0, K_c - 1 < 0$  ( $U, W > 0, U = 2W$ ) separates two different insulating (charge gapped) sectors of the phase diagram: for  $U > \max\{2W, 0\}$ ,  $m_c < 0$ ,  $M_c \rightarrow -\infty$  and therefore the  $\varphi_c$  field gets ordered with vacuum expectation value  $\langle \varphi_c \rangle = 0$ ; for  $2W > \max\{U, 0\}$   $m_c > 0$   $M_c \rightarrow +\infty$  and therefore the  $\varphi_c$  field gets ordered with vacuum expectation value  $\langle \varphi_c \rangle = \sqrt{\pi/8K_c}$ .

Away from half-filling the charge sector is gapless and is described by the free massless Bose field (25). The corresponding correlations (34)-(35) show a power law decay at large distances with critical indices determined by the bare value of the coupling constant  $K_c$  (27). The spin channel remains massive at  $U + 2W < 0$  and gapless for  $U + 2W \geq 0$ .

## B. Correlation functions

To clarify the symmetry properties of the ground states of the system in different sectors we introduce the following set of order parameters describing the short wavelength fluctuations of the site-located charge and spin density

$$\begin{aligned} \Delta_{CDW}(n) &= e^{i2\pi\nu n} \sum_{\sigma} \hat{\rho}_{\sigma}(n) \rightarrow \\ \begin{cases} \sin(\sqrt{2\pi K_c} \varphi_c(x)) \cos(\sqrt{2\pi K_s} \varphi_s(x)), & \text{at } \nu = 1/2 \\ e^{i\sqrt{2\pi K_c} \varphi_c(x)} \cos(\sqrt{2\pi K_s} \varphi_s(x)), & \text{at } \nu \neq 1/2 \end{cases} \end{aligned} \quad (38)$$

$$\begin{aligned} \Delta_{SDW}(n) &= e^{i2\pi\nu n} \sum_{\sigma} \sigma \hat{\rho}_{\sigma}(n) \rightarrow \\ \begin{cases} \cos(\sqrt{2\pi K_c} \varphi_c(x)) \sin(\sqrt{2\pi K_s} \varphi_s(x)), & \text{at } \nu = 1/2 \\ e^{i\sqrt{2\pi K_c} \varphi_c(x)} \sin(\sqrt{2\pi K_s} \varphi_s(x)), & \text{at } \nu \neq 1/2 \end{cases} \end{aligned} \quad (39)$$

and two superconducting order parameters corresponding to singlet ( $\Delta_{SS}$ ) and triplet ( $\Delta_{TS}$ ) superconductivity:

$$\begin{aligned} \Delta_{SS}(x) &= R_{\uparrow}^{\dagger}(x) L_{\downarrow}^{\dagger}(x) - R_{\downarrow}^{\dagger}(x) L_{\uparrow}^{\dagger}(x) \rightarrow \\ \exp\left(i\sqrt{\frac{2\pi}{K_c}} \theta_c(x)\right) \cos(\sqrt{2\pi K_s} \varphi_s(x)), \end{aligned} \quad (40)$$

$$\begin{aligned} \Delta_{TS}(x) &= R_{\uparrow}^{\dagger}(x) L_{\downarrow}^{\dagger}(x) + R_{\downarrow}^{\dagger}(x) L_{\uparrow}^{\dagger}(x) \rightarrow \\ \exp\left(i\sqrt{\frac{2\pi}{K_c}} \theta_c(x)\right) \sin(\sqrt{2\pi K_s} \varphi_s(x)). \end{aligned} \quad (41)$$

In the particular case of a half-filled band, we consider an additional pair of order parameters, corresponding to the short wavelength fluctuations of the bond-located charge and spin density

$$\begin{aligned} \Delta_{Dimer}(n) &= (-1)^n \sum_{\sigma} (\hat{q}_{\sigma}(n) + \hat{q}_{\sigma}^{\dagger}(n)) \rightarrow \\ \cos(\sqrt{2\pi K_c} \varphi_c(x)) \cos(\sqrt{2\pi K_s} \varphi_s(x)), \end{aligned} \quad (42)$$

$$\begin{aligned} \Delta_{Bd-SDW}(n) &= (-1)^n \sum_{\sigma} \sigma (\hat{q}_{\sigma}(n) + \hat{q}_{\sigma}^{\dagger}(n)) \rightarrow \\ \sin(\sqrt{2\pi K_c} \varphi_c(x)) \sin(\sqrt{2\pi K_s} \varphi_s(x)), \end{aligned} \quad (43)$$

With these results for the excitation spectrum and the behavior of the corresponding fields Eqs. (34)-(36) we now discuss the *weak-coupling* ground state phase diagram of the model (3).

## C. The half-filled band case.

At half-filling the weak-coupling phase diagram of the PKH model consists of the following sectors (see Fig.2).

- A. The Singlet Superconducting sector:  
 $U < 0$  and  $W < 0$ ;  
 $M_s \neq 0$ ,  $\langle \varphi_s \rangle = 0$ ;  $M_c = 0$ ,  $K_c^* > 1$ .

This sector of the coupling constants corresponds to the strong-coupling regime in the spin-channel and gapless charge channel. The dynamical generation of a spin gap accompanied by the ordering of the field  $\varphi_s$  with vacuum expectation value  $\langle \varphi_s \rangle = 0$  leads to a complete suppression of the SDW, Bd-SDW, and TS instabilities.

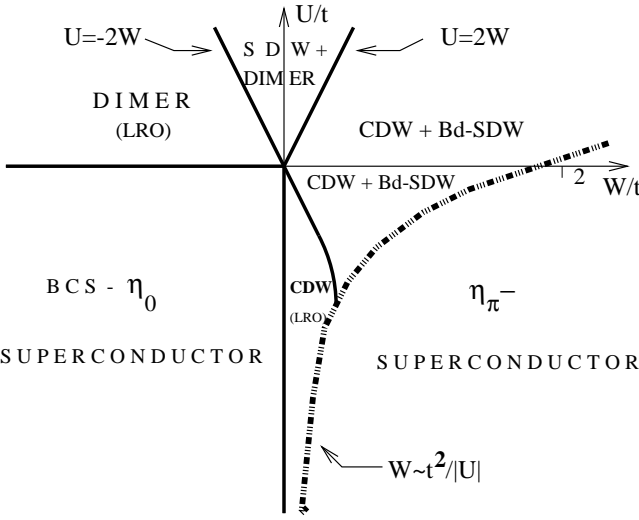


FIG. 2. The groundstate phase diagram of the 1D Penson-Kolb-Hubbard model at half-filling. The dot-dashed line marks a transition into the  $\eta_\pi$ -superconducting phase. Solid lines separate different phases: 1. Dimer - long range ordered (LRO) dimerized (Peierls) phase. 2. CDW - LRO charge density wave phase; 3. SDW + Dimer - insulating phase with an identical power-law decay of spin-density-wave and Peierls correlations. 4. CDW + Bd-SDW - insulating phase with an identical power-law decay of CDW and bond-located SDW correlations. 5. BCS -  $\eta_0$ -superconductor - singlet superconducting phase exhibiting a continuous evolution with increasing  $|U|/t$  and/or  $|W|/t$  from the standard BCS limit into the local pair  $\eta_0$  state.

The CDW, Dimer, and SS instabilities survive and show a power-law decay at large distances

$$\langle \Delta_{CDW}(x)\Delta_{CDW}(x') \rangle \sim \langle \Delta_{Dimer}(x)\Delta_{Dimer}(x') \rangle \sim |x-x'|^{-K_c^*}, \quad (44)$$

$$\langle \Delta_{SS}(x)\Delta_{SS}(x') \rangle \sim |x-x'|^{-1/K_c^*}. \quad (45)$$

where  $K_c^*$  is the fixed-point value of the parameter  $K_c$ . For  $U, W < 0$ ,  $K_c^* > 1$  and the SS instability dominates in the groundstate.

Note that, at  $W = 0$  or  $U = 0$ ,  $K_c^* = 1$  and the CDW, Dimer, and SS correlations show an identical power law decay at large distances. At  $W = 0$  coexistence of the CDW and superconducting instabilities in the ground state reflects the high  $SU(2) \otimes SU(2)$  symmetry of the 1/2-filled Hubbard model [39]. In the case of the Penson-Kolb model ( $U = 0$ ), due to the charge- $U(1)$  symmetry of the pair-hopping term, there is no symmetry reason which guarantees scaling to the  $SU(2)$  invariant fixed point  $K_c^* = 1$ . As it was shown by Affleck and Marston, the higher order RG corrections give  $K_c^* > 1$  indicating the dominating character of the SS instability in the

ground state of the 1/2-filled PK model for arbitrary  $W < 0$  [26].

#### B. The CDW sector:

$$U < 0, 0 < W < -U/2.$$

$$M_s \neq 0, \langle \varphi_s \rangle = 0; M_c \neq 0, \langle \varphi_c \rangle = \sqrt{\pi/8K_c}.$$

For  $W > 0$  the commensurability gap in the charge degrees of freedom opens. For  $0 < W < -U/2$  the spin sector remains massive. Ordering of the field  $\varphi_s$  with vacuum expectation value  $\langle \varphi_s \rangle = 0$  leads to a complete suppression of the SDW, Bd-SDW, and TS instabilities. Ordering of the field  $\varphi_c$  with vacuum expectation value  $\langle \varphi_c \rangle = \sqrt{\pi/8K_c}$  leads to a suppression of the SS and Dimer correlations. The CDW correlations show a true long-range order

$$\langle \Delta_{CDW}(x)\Delta_{CDW}(x') \rangle \sim const \quad (46)$$

in the ground state. Therefore in this sector of the phase diagram the system displays the properties of the CDW insulator.

#### C. The Peierls (dimerized) sector:

$$U > 0, 0 < U < -2W.$$

$$M_s \neq 0, \langle \varphi_s \rangle = 0; M_c \neq 0, \langle \varphi_c \rangle = 0.$$

Ordering of the field  $\varphi_s$  with vacuum expectation value  $\langle \varphi_s \rangle = 0$  leads to a complete suppression of the SDW, Bd-SDW, and TS instabilities. Ordering of the field  $\varphi_c$  with vacuum expectation value  $\langle \varphi_c \rangle = 0$  leads to a suppression of the SS and CDW correlations. The Dimer correlations show a true long-range order

$$\langle \Delta_{Dimer}(x)\Delta_{Dimer}(x') \rangle \sim const \quad (47)$$

in the ground state. Therefore in this sector of the phase diagram the system is a dimerized (Peierls) insulator.

#### D. The (CDW + Bd-SDW) sector:

$$W > 0, -2W < U < 2W.$$

$$M_s = 0, K_s^* = 1, M_c \neq 0, \langle \varphi_c \rangle = \sqrt{\pi/8K_c}.$$

The generation of a gap in the charge excitation spectrum, accompanied by the ordering of the field  $\varphi_c$  with vacuum expectation value  $\langle \varphi_c \rangle = \sqrt{\pi/8K_c}$  leads to a suppression of the superconducting, SDW, and Dimer ordering. The CDW and Bd-SDW correlations show a power-law decay at large distances

$$\begin{aligned} \langle \Delta_{CDW}(x)\Delta_{CDW}(x') \rangle &\sim \langle \Delta_{Bd-SDW}(x)\Delta_{Bd-SDW}(x') \rangle \\ &\sim |x-x'|^{-1}. \end{aligned} \quad (48)$$

Therefore this sector of the phase diagram corresponds to the insulating phase with coexisting CDW and Bd-SDW instabilities.

#### E. The (SDW + Dimer) sector:

$$U > 2|W|.$$

$$M_s = 0, K_s^* = 1, M_c \neq 0, \langle \varphi_c \rangle = 0.$$

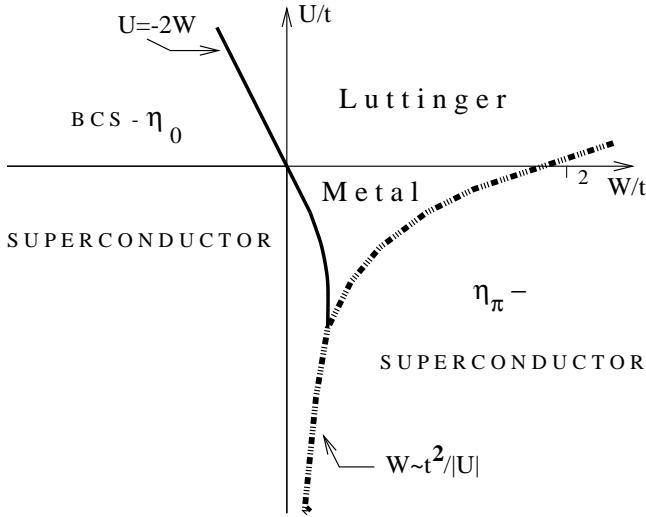


FIG. 3. The ground state phase diagram of the 1D Penon-Kohb-Hubbard model for  $\nu \neq 1/2$ . The dot-dashed line marks the transition into the  $\eta_\pi$ -superconducting phase. The solid line separates the superconducting phase from the Luttinger metal phase characterized by an identical power-law decay of the SDW, CDW, Bd-SDW, and Dimer correlations.

The generation of a gap in the charge excitation spectrum, accompanied by the ordering of the field  $\varphi_c$  with vacuum expectation value  $\langle \varphi_c \rangle = 0$  leads to a suppression of the superconducting, CDW, and Bd-SDW correlations. The SDW and Dimer correlations show a power-law decay at large distances

$$\begin{aligned} \langle \Delta_{SDW}(x) \Delta_{SDW}(x') \rangle &\sim \langle \Delta_{Dimer}(x) \Delta_{Dimer}(x') \rangle \\ &\sim |x - x'|^{-1}. \end{aligned} \quad (49)$$

Therefore this sector of the phase diagram corresponds to the antiferromagnetic insulating phase with coexisting SDW and Peierls instabilities.

### 1. The non-half-filled band case.

Away from half-filling and for  $U < 0$  the weak-coupling phase diagram of the PKH model consists of the following two sectors.

#### A1. The SS sector:

$$U + 2W < 0.$$

$$M_s \neq 0, \langle \varphi_s \rangle = 0; M_c = 0, K_c > 1.$$

In this sector of coupling constants the SDW, Bd-SDW, and TS instabilities are suppressed. The CDW, Dimer, and SS instabilities show a power-law decay at large distances

$$\begin{aligned} \langle \Delta_{CDW}(x) \Delta_{CDW}(x') \rangle &\sim \langle \Delta_{Dimer}(x) \Delta_{Dimer}(x') \rangle \\ &\sim |x - x'|^{-K_c}, \end{aligned} \quad (50)$$

$$\langle \Delta_{SS}(x) \Delta_{SS}(x') \rangle \sim |x - x'|^{-1/K_c}. \quad (51)$$

As it follows from (27), for  $U = 2W < 0$ ,  $K_c > 1$  and the SS instability dominates in the groundstate.

#### B1. The metallic Luttinger-liquid sector:

$$U + 2W \geq 0.$$

$$M_s = 0, K_s^* = 1, M_c = 0, K_c < 1.$$

Both the charge and the spin excitations are gapless. All correlations show a power-law decay in the infrared limit. However, as far as  $K_c < 1$ , the superconducting correlations

$$\begin{aligned} \langle \Delta_{SS}(x) \Delta_{SS}(x') \rangle &\simeq \langle \Delta_{TS}(x) \Delta_{TS}(x') \rangle \\ &\sim |x - x'|^{-1-1/K_c} \end{aligned} \quad (52)$$

decay faster than the density-density correlations

$$\langle \Delta_i(x) \Delta_i(x') \rangle \sim |x - x'|^{-1-K_c}, \quad (53)$$

where  $i \equiv \text{CDW,SDW,Dimer,Bd-SDW}$ . Therefore in this sector the ground state of the PKH model shows properties of the Luttinger liquid phase with a weakly dominating tendency towards the density-density type ordering.

To summarize this section, we have presented the weak-coupling groundstate phase diagram for one-dimensional PKH model for arbitrary  $U$  and  $W$  ( $|U|, |W| \ll t$ ). We have shown that the model has a very rich phase diagram including at half-filling, the singlet-superconducting phase ( $U, W < 0$ ) and four different insulating phases corresponding to the Mott antiferromagnet ( $U > 2|W|$ ), the Peierls dimerized insulator ( $0 < U < -2W$ ) and the CDW insulator ( $W > 0, U < -2W$ ) and an unconventional insulating phase characterized by the coexistence of the CDW and the bond-located staggered magnetization Bd-SDW ( $W > 0, U < 2|W|$ ). The possibility of bond-located ordering results from the site-off-diagonal nature of the pair-hopping term and is a special feature of the half-filled band case. Away from half-filling the phase diagram consists of the singlet-superconducting phase ( $U + 2W < 0$ ) and the metallic Luttinger-liquid phase ( $U + 2W > 0$ ).

Note the absence of the  $\eta_\pi$ -superconducting phase in the weak-coupling phase diagram. This results from the finite-band nature of the transition into an  $\eta_\pi$ -paired phase [27]. Therefore in the used infinite-band bosonization approach, such a transition could not be traced. In the forthcoming section we will use exact Lanczos diagonalizations for chains up to  $L = 12$  sites to study in detail the nature of the transition into the  $\eta_\pi$ -superconducting phase.

## IV. NUMERICAL STUDIES

In this section we study the nature of the transition into the  $\eta_\pi$ -superconducting phase using exact diagonalizations for chains up to  $L = 12$  sites.

### A. The half-filled band case

We start with the  $W/t$  dependence of the groundstate energy for different  $U \leq 0$ .

In Fig. 4a we have plotted the groundstate energy ( $E_{GS}$ ) shifted by  $\frac{1}{2}N_e|U|$  of the  $L = 10$  chain at half-filling as a function of  $W/t$ , for selected values of  $U/t$ . We clearly observe a different behavior of the groundstate energy for  $W > 0$  and  $W < 0$ . For  $W < 0$  the ground state energy continuously approaches the XY model in the limit  $|W| \rightarrow \infty$ . There is no trace of any additional transition for  $W < 0$ , in agreement with the density-matrix renormalization group (DMRG) results for  $U = 0$  [29]. However, for  $W > 0$ , the groundstate energy shows a non-monotonic behaviour. We observe that above some critical value of the pair-hopping coupling  $W_c$  the energy is already almost linear in  $W$  and approaches the groundstate energy of the XY model. Hence for  $W > W_c$  the *one particle hopping term is almost frozen out*. This change of behaviour is attributed to the transition to the  $\eta_\pi$ -superconducting state [27]. The accurate definition for  $W_c$  will be given below; however, the numerical data presented in Fig. 4a already clearly indicate the renormalization of the critical value of the pair-hopping coupling  $W_c$  by the on-site Hubbard attraction. At  $U = 0$   $W_c \simeq 1.8t$  [27] and it reduces to  $W_c \simeq 0.4t$  at  $U/t = -8$ .

Another way to visualize this transition is to show the pairing phenomenon in real space. The corresponding quantity is the expectation value to find an on-site pair and is given by

$$P_{rs} = \frac{1}{L} \sum_{n=1}^L \langle \rho_{n\uparrow} \rho_{n\downarrow} \rangle. \quad (54)$$

$P_{rs}$  is shown in Fig. 4b. For  $W < 0$  the pairs appear continuously in the system. In the opposite case  $W > 0$ ,  $W \ll t$  and  $|U| < 4t$  the tendency to pairing is even reduced. This “effective repulsive” character is absent for  $U < -4t$ , but remains up to  $W < 0.8t$  for  $U = 0$  and up to  $W < 0.4t$  for  $U = -2t$ . We attribute this behaviour to a finite size effect where the energy scale coming from the exponentially small charge gap in  $W/t$  is not traced in the  $L = 10$  chain. For  $U < -4t$  the tendency to pairing is present for  $W > 0$ . As is seen from Fig. 4b for arbitrary  $U < 0$ , the almost fully paired state is realized in the ground state of the half-filled PKH model for a *finite* value of the pair-hopping amplitude  $W > W_c$ . However, it should be stressed that due to the quasi-bosonic character of the pairs, the weight of unpaired particles remains *extremely small but finite* even for  $W \gg W_c$ . The critical value of the pair-hopping amplitude corresponding to the transition into an  $\eta_\pi$ -superconducting state  $W_c$  is straightforward to find when the number of electrons is  $N_e = 2(2n + 1)$ . The level crossing phenomenon is generic in this case. In Fig. 5a we have plotted the lowest energy levels (LEL) in each sectors  $Q_{tot} = 0$  and  $Q_{tot} = \pi$  as a function of  $W/t$  in

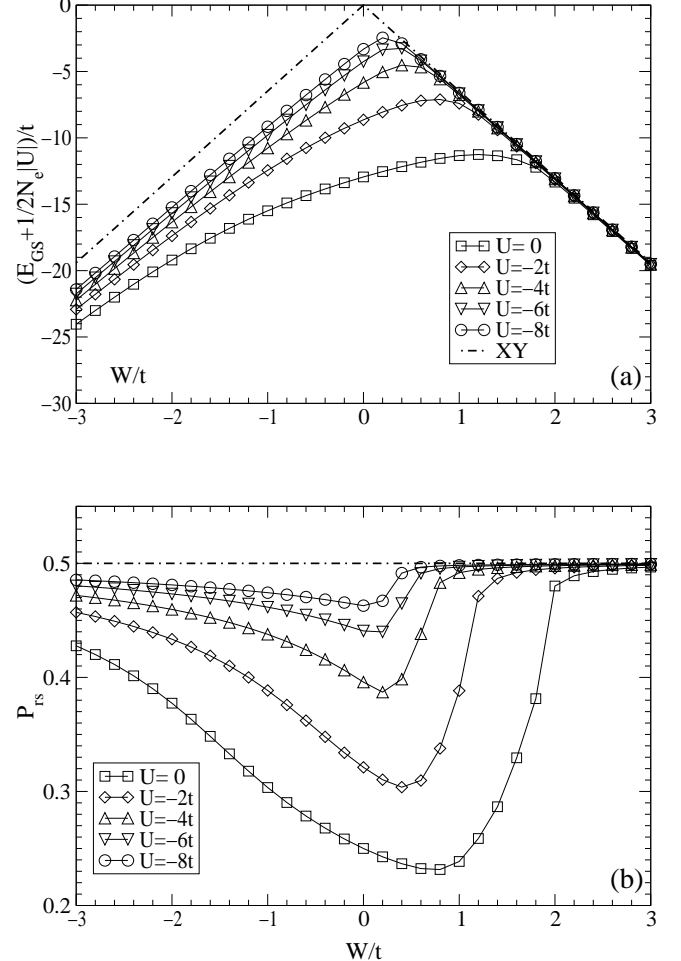


FIG. 4. Groundstate energy ( $E_{GS}$ ) shifted by  $\frac{1}{2}N_e|U|$  (a) and real space pairing probability  $P_{rs}$  (b) of the  $L = 10$  chain at half-filling, as a function of  $W/t$ , for  $U/t = 0, -2, -4, -6, -8$ . The corresponding symbols are indicated in the figure. The dot-dashed line in (a) represents the groundstate energy of the spin- $\frac{1}{2}$  XY model corresponding to the limiting case  $|W|/t, |U|/t \rightarrow \infty$ .

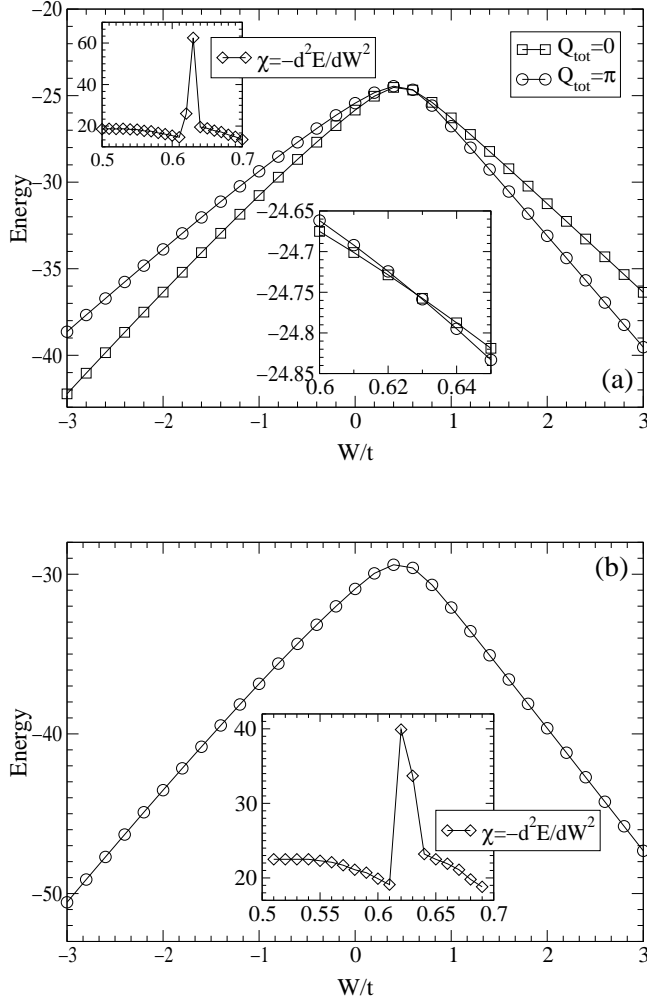


FIG. 5. (a) Lowest energy vs.  $W/t$  calculated in the  $Q_{tot} = 0$  (open squares) and  $Q_{tot} = \pi$  (open circles) subspaces in the case of a half-filled  $L = 10$  chain at  $U/t = -4$ . The insets in (a) show the level crossing and singularity in the generalized stiffness  $\chi(W) = -\partial^2 E_0(W)/\partial W^2$  at  $W_c \simeq 0.625t$ . (b) Groundstate energy vs.  $W/t$  for a half-filled  $L = 12$  chain at  $U/t = -4$ . The inset in (b) shows the singularity in  $\chi(W)$ .

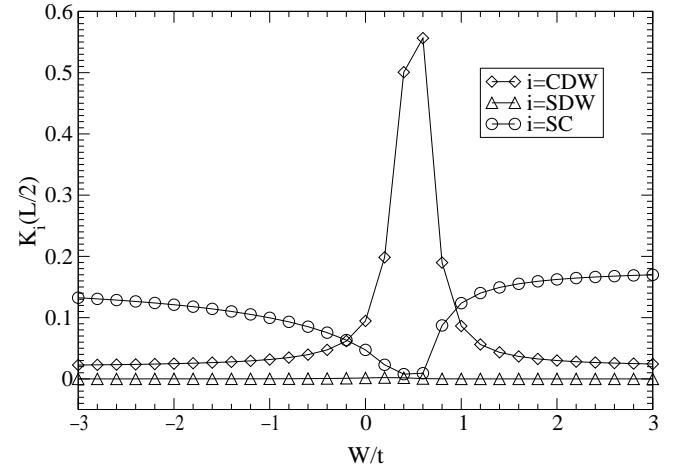


FIG. 6. Correlation functions  $K_i(r = L/2)$  ( $i = \text{CDW}, \text{SDW}, \text{SC}$ ) vs.  $W/t$  for the half-filled PKH chain ( $L = 10$ ) at  $U = -4t$ . The corresponding symbols are indicated in the figure.

the case of a half-filled  $L = 10$  chain and for  $U/t = -4$ . Indeed, in this case we observe a well defined transition from the  $Q = 0$  to the  $Q = \pi$  sector at  $W_c = 0.625t$ . At the same value we observe (see inset in Fig. 5a) a singularity in the behaviour of the generalized stiffness (GS)

$$\chi(W) = -\partial^2 E_0 / \partial W^2|_{U=const}$$

due to the presence of a kink in the ground state energy  $E_0(W)$  at the point where the LEL in sectors  $Q_{tot} = 0$  and  $Q_{tot} = \pi$  cross each other. When the number of electrons is  $N_e = 4n$  the ground state of the system always remains in the sector of momentum space with  $Q_{tot} = 0$ . In Fig. 5b we have plotted the ground state energy of the half-filled PKH model for  $L = 12$ . The insets show the anomaly in the behaviour of the generalized stiffness  $\chi(W)$  at the same value  $W_c = 0.625t$  as in the case of  $L = 10$  chain. This clearly indicates the irrelevance of the finite-size effects already for  $L = 10$  in the considered case  $U/t = -4$ . We define the critical value of the pair-hopping amplitude corresponding to the transition into the  $\eta_\pi$ -paired state at the point where  $\chi$  exhibits a singularity.

To investigate the nature of ordering in the different phases we study the behaviour of the correlation functions. In Fig. 6 we plotted the absolute values of the spin-spin correlator

$$K_{SDW}(r) = \frac{1}{L} \sum_n \langle S^z(n) S^z(n+r) \rangle, \quad (55)$$

the density-density correlator

$$K_{CDW}(r) = \frac{1}{L} \sum_n (-1)^n \langle \hat{\rho}(n) \hat{\rho}(n+r) \rangle, \quad (56)$$

where  $\hat{\rho}(n) = \sum_{\sigma} \hat{\rho}_{\sigma}$  and the superconducting correlator

$$K_{SC}(r) = \frac{1}{L} \sum_n \langle \eta_0^{\dagger}(n) \eta_0(n+r) \rangle \quad (57)$$

at  $r = L/2$  for different values of  $W/t$  for the half-filled  $L = 10$  PKH chain at  $U = -4t$ . We clearly observe the existence of two superconducting phases separated by a phase with dominating density-density correlations. In contrast to generalized stiffness the finite-size effects in correlation functions are sufficiently strong for  $L = 10$  to use the large-distance properties of the correlation functions for the precise determination of the  $W_c$ . However, already in the case of the  $L = 10$  chain the essential physical details of the phase diagram are completely transparent.

In order to clarify the nature of the superconducting phases corresponding to  $W > 0$  and  $W < 0$  respectively, we show in Fig. 7 the superconducting correlator  $K_{SC}(r)$  (a) and the momentum space pairing probability  $P_{ms}(Q) = \langle A_Q^{\dagger} A_Q \rangle$  (b) as a function of  $W/t$ , for  $U/t = -4$  for the  $L = 10$  chain at half-filling.

For  $W < 0$   $K_{SC}(r)$  smoothly increases with increasing  $|W|/t$ . The distribution  $P_{ms}(Q)$  has a peak at  $Q = 0$ . The weight of this peak continuously increases with  $|W|/t \rightarrow \infty$ . The probability to find a  $\pi$ -pair is almost zero. The inset in Fig. 7a shows  $K_{SC}(r)$  at  $W/t = -2.6$  (open symbols). At  $W/t = -2.6$  the superconducting correlations are well established and show weak decay with distance. In the opposite case,  $W > 0$ ,  $K_{SC}(r)$  and  $P_{ms}(Q = 0)$  continuously decrease. The superconducting correlations are completely suppressed at  $0.4t < W < W_c \simeq 0.75t$ . The expectation value to find a Cooper pair with center-of-mass momentum  $Q = 0$  becomes almost zero at  $W > W_c$ . However at  $W > W_c$  we observe a drastic change of  $K_{SC}(r)$  and  $P_{ms}(Q)$ . The superconducting correlations strongly increase and the strong peak at  $Q = \pi$  appears spontaneously in the distribution  $P_{ms}(Q)$ . The probability to find a Cooper pair with center-of-mass momentum  $Q = \pi$  quickly approaches its limiting value corresponding to the case  $W/t \rightarrow \infty$ . The inset in Fig. 7a shows  $K_{SC}(r)$  at  $W/t = 2.6$  (filled symbols). At  $W/t = 2.6$  the superconducting correlations are slightly stronger than at  $W/t = -2.6$  and clearly show alternating behaviour with periodicity of two lattice spacing. The data presented in Fig. 7 clearly show the  $\eta_{\pi}$  ordering at  $W > W_c$ .

## B. The non-half-filled band case

In Fig. 8 we have plotted  $P_{rs}$  as a function of  $W/t$  for various values of the parameter  $U/t$  calculated for the  $L = 12$  chain and two particular band fillings  $\nu = 1/4$  and  $\nu = 1/3$ . As we see the transition into the  $\eta_{\pi}$ -paired state occurs also away from half-filling. Moreover, in contrast to the half-filled case, the transition is now very sharp.

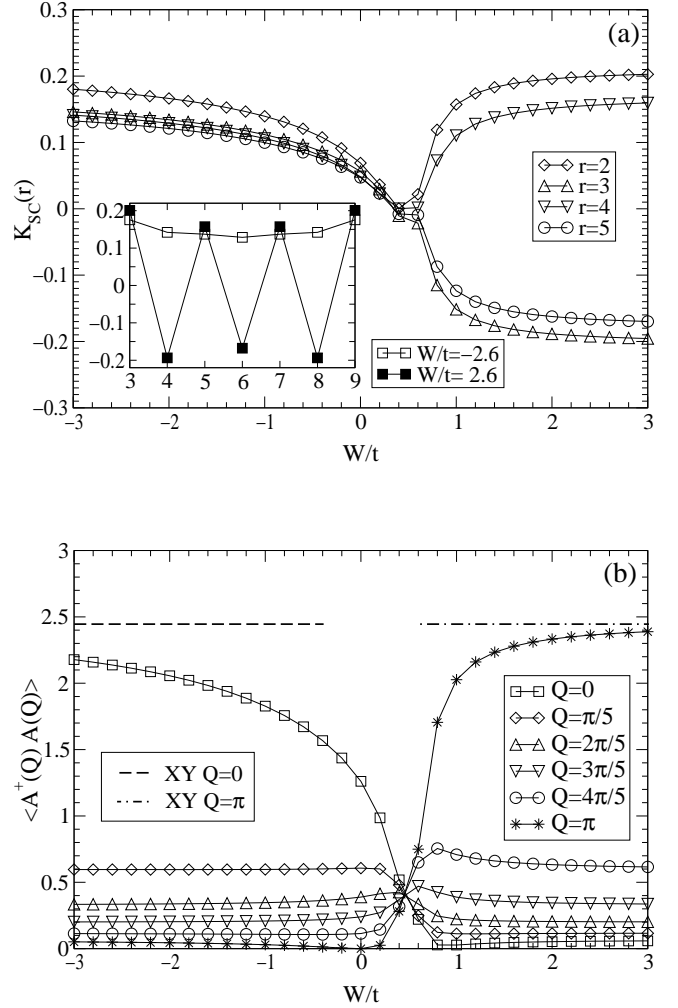


FIG. 7. The superconducting correlator  $K_{SC}(r)$  (a) and the distribution  $P_{ms}(Q) = \langle A_Q^{\dagger} A_Q \rangle$  (b) vs.  $W/t$  for the half-filled PKH chain ( $L = 10$ ) at  $U/t = -4$ . The inset in (a) shows  $K_{SC}(r)$  at  $W/t = -2.6$  (open symbols) and  $W/t = 2.6$  (filled symbols). The dashed and dashed-dotted lines in (b) correspond to maximum values approached by the distribution  $P_{ms}(Q)$  for  $Q = 0$  and  $Q = \pi$  in the limiting case  $|W|/t, |U|/t \rightarrow \infty$ .

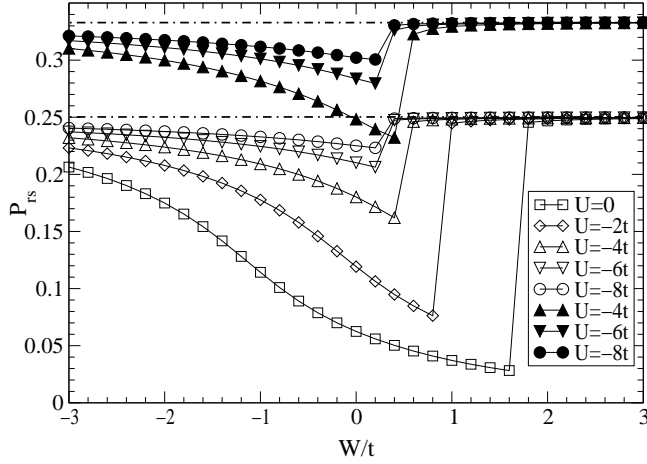


FIG. 8. Real space pairing probability  $P_{rs}$  vs.  $W/t$  and various values of the parameter  $U/t$  for  $L = 12$ ,  $N_e = 6$  (open symbols) and  $N_e = 8$  (filled symbols).

To study the phase diagram at  $\nu \neq 1/2$  we investigate the behaviour of the CDW and SC correlations. In Fig. 9a we have plotted the correlators  $K_{CDW}$  and  $K_{SC}$  at  $r = L/2$  vs.  $W/t$  calculated for the  $L = 12$  PKH chain in the case of  $\nu = 1/3$  and various values of the parameter  $U/t$ . As it follows from the behaviour of the correlation functions the sector with dominating density-density instability shrinks to a narrow strip with increasing on-site attraction. If for  $U/t = -4$  the density-density correlations still dominate for  $W \simeq 0.4t$ , for  $U/t = -6$  only superconducting correlations remain.

In Fig. 9b we show the same correlators calculated for a fixed on-site attraction  $U/t = -4$  and two different band fillings  $\nu_1 = 1/4$  and  $\nu_2 = 1/3$ . As it is clearly seen the decreasing band filling leads to a reduction of the range of coupling constants where the system shows non-superconducting behaviour. In agreement with the strong-coupling expansion analysis of Sect. II we conclude that the system exhibits a transition from the BCS type singlet superconducting phase at  $W < W_c$  into an  $\eta_\pi$  paired state at  $W > W_c$ .

### C. Nature of the transition

In order to show the finite bandwidth nature of the transition into an  $\eta_\pi$ -superconducting state in Fig. 10 we have plotted the momentum distribution

$$\langle n_k \rangle = \sum_{\sigma} \langle c_{k\sigma}^\dagger c_{k\sigma} \rangle$$

in the ground state of the  $L = 10$  half-filled PKH chain as a function of the parameter  $W/t$  at  $U/t = -4$ . In the case of an attractive Hubbard model ( $W = 0, U = -4t$ ) the momentum distribution in the groundstate has a

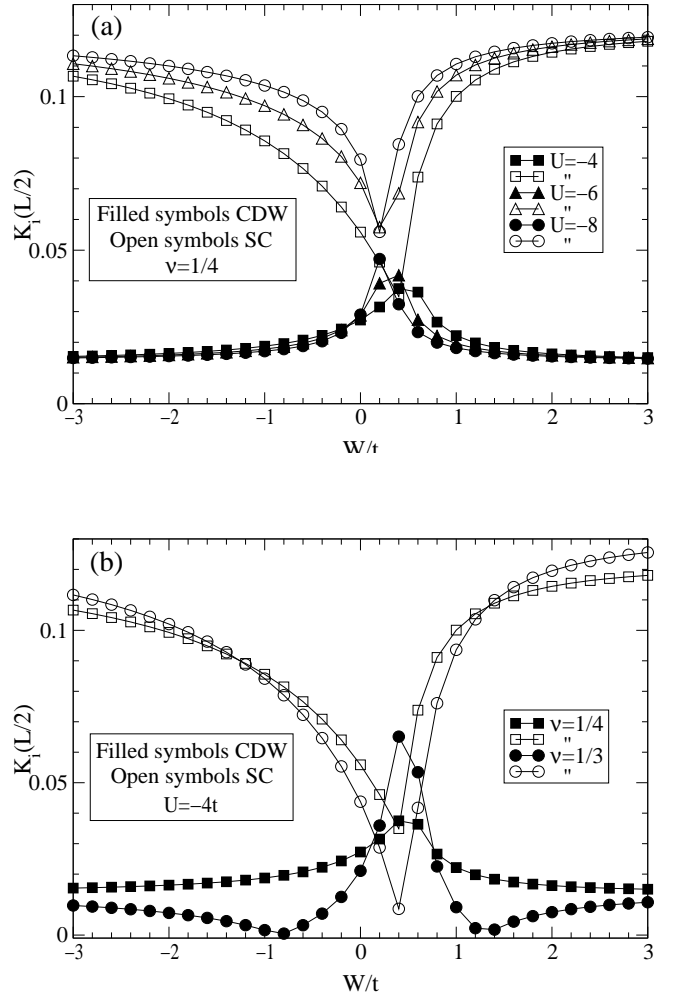


FIG. 9. Correlation functions  $K_{CDW}(r = L/2)$  (filled symbols) and  $K_{SC}(r = L/2)$  (open symbols) for the  $L = 12$  chain,  $\nu = 1/4$  and  $U/t = -4, -6, -8$  (a) and for the  $L = 12$  chain,  $U/t = -4$  and  $\nu = 1/4$  (squares) and  $\nu = 1/3$  (circles) (b).

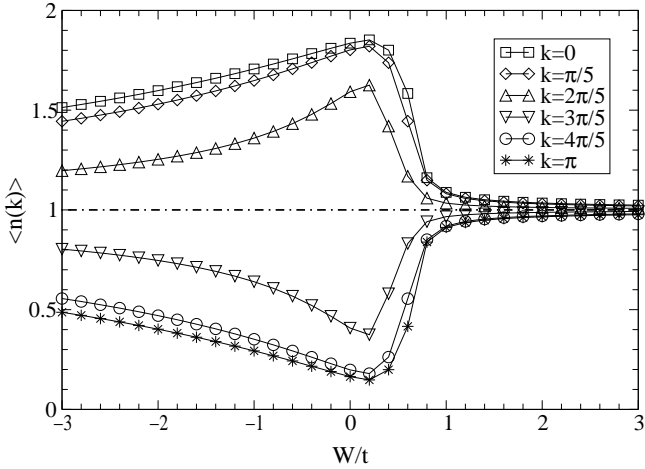


FIG. 10.  $\langle n_k \rangle$  distribution for different values of the parameter  $W/t$ , in the case of half-filled  $L = 10$  chain and for  $U/t = -4$ . The corresponding symbols are indicated in the figure.

shape of the standard Fermi distribution: the states with  $|k| < k_F = \pi/2$  are almost completely occupied, while the states with  $|k| > k_F = \pi/2$  are almost empty. In the case of  $W < 0$  the momentum distribution remains qualitatively unchanged. With increasing  $|W|/t$  the distribution  $\langle n_k \rangle$  in a monotonic way approaches its limiting behaviour  $\langle n_k \rangle = 1$  at  $|W|/t \rightarrow \infty$ .

At  $W > 0$  the standard shape in the momentum distribution remains for  $0 < W < W_c$ ; however, at  $W \simeq W_c \simeq 0.625t$  we observe an abrupt change in the momentum distribution. For  $W > W_c$   $\langle n_k \rangle \simeq 1$  for all  $k$ . States with different momenta are almost equally occupied by electrons. There is no trace of the Fermi distribution. As far as states with momentum  $k$  and  $\pi - k$  are almost equally occupied after the transition, the contribution of the *one-electron band* to the groundstate energy is almost *completely suppressed*. The ground state energy of the system becomes linear in  $W$ . Therefore we conclude that the transition into an  $\eta_\pi$ -superconducting state corresponds to *destruction of the single-electron conduction band* and the *creation of a strongly-correlated  $\eta_\pi$ -pair band*.

As far as the transition into an  $\eta_\pi$ -paired state is connected with the formation of a  $\eta_\pi$ -pair (doublon) band, after the transition the characteristic length scale in the system  $\xi \simeq 0$ . Therefore the finite-size effects are very weak. In Fig. 11 we have plotted  $W_c$  vs.  $U$  calculated for the half-filled chain with  $L = 6, 8, 10, 12$ . As it can be seen in this figure the finite size effects have only a *very weak* influence on the critical value.

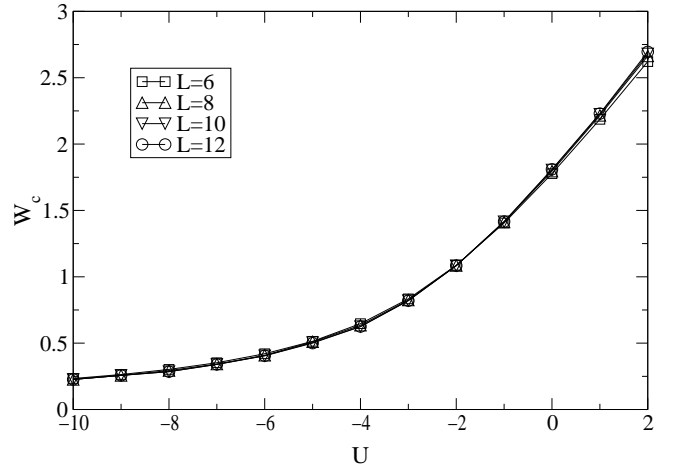


FIG. 11.  $W_c$  vs.  $U$  calculated for the half-filled PKH chain with  $L = 6, 8, 10, 12$ .

## V. SUMMARY

To summarize, in this paper we have studied the groundstate phase diagram of the one-dimensional Penson-Kolb-Hubbard model using the continuum-limit field theory approach and finite system numerical studies. We have shown that the model has a very rich phase diagram including, at half-filling (see Fig.2), two different superconducting phases and four different insulating phases corresponding to the singlet superconducting phase ( $U, W < 0$ ) with BCS type pairing at  $|U|, |W| \ll t$ , monotonically evolving into the local-pair  $\eta_0$ -superconducting phase with  $U/t$  and/or  $W/t$  approaching  $-\infty$ ; the  $\eta_\pi$ -superconducting phase ( $W > W_c(U) > 0$ ); the Mott antiferromagnet ( $U > 2|W|$ ) phase, the Peierls dimerized insulator ( $0 < U < -2W$ ); the CDW insulator ( $W > 0, U < -2W$ ); the unconventional insulating phase characterized with coexistence of the CDW and bond-located staggered magnetization Bd-SDW ( $W > 0, U < 2|W|$ ).

Away from half-filling (see Fig.3) the phase diagram consists of the singlet-superconducting phase ( $W < \min\{-U/2, W_c(U)\}$ ), and the metallic Luttinger-liquid (LL) phase ( $-U/2 < W < W_c(U)$ ), and the  $\eta_\pi$ -superconducting phase ( $W > W_c(U) > 0$ ). With increasing on-site attraction the LL phase shrinks and at a critical value  $U_c$ , determined by the condition  $U_c + 2W_c(U_c) = 0$ , only the critical line  $W_c(U)$  remains for  $U < U_c$ . In this range of couplings the transition from an  $\eta_0$ -superconductor to an  $\eta_\pi$ -superconductor is realized. The critical value  $W_c(U)$  weakly depends on the band filling displaying a non-monotonic behaviour: at  $|U|/t \ll 1$  a slight decrease while at  $|U|/t \gg 1$  a slight increase with increasing  $\nu$ .

The obtained phase diagram is in agreement with results of previous studies based on the real space renormal-

ization group method [28], the continuum-limit approach [36], the slave-boson mean-field method [37] as well as for the particular case of  $U = 0$  with the results of numerical studies using exact (Lanczos) diagonalizations [27] and DMRG studies [29].

Using Lanczos diagonalization we have studied in detail the transition into the  $\eta_\pi$ -paired state. After the transition the on-site pairing probability sharply approaches its limiting value corresponding to the case  $W/t \rightarrow \infty$  and the  $\eta_\pi$ -superconducting correlations dominate in the system. The transition corresponds to an abrupt change in the groundstate structure. After the transition the single-electron conduction band is completely destroyed and the strongly-correlated  $\eta_\pi$ -pair (doublon) band is established. The transition occurs at any band filling, the critical value  $W_c(U)$  *weakly depends on the band filling* but is strongly renormalized by the on-site Hubbard interaction:  $W_c(U)$  is linear in  $U$  for  $|U|/t$  of the order of unity and is inversely proportional to  $|U|$  i.e  $W_c(U) \simeq -t^2/|U|$  for  $|U|/t \gg 1$ . We believe that this phase diagram is generic for the Penson-Kolb-Hubbard model and will remain unchanged in higher dimensions.

This work was partially supported by the DFG through SP 1073. G.J. was partially supported by the INTAS-Georgia grant N 97-1340. M.S acknowledges the hospitality at the Institute of Physics, University of Augsburg, where part of this work was performed.

- [7] P. Nozieres and S. Schmitt-Rink, *J. Low Temp. Phys.*, **59**, 195 (1985).
- [8] S. Robaszkiewicz, R. Micnas, and K.A. Chao, *Phys. Rev. B* **23**, 1447, (1981).
- [9] R. Frésard, B. Glaser, and P. Wölfle, *J. Phys.: Condens. Matter* **4**, 8565 (1992).
- [10] R. Housmann, *Z. Phys. B* **91**, 291 (1993); *Phys. Rev. B* **49**, 12975 (1994).
- [11] M. Randeria, N. Trivedi, A. Moreo, and R.T. Scalettar, *Phys. Rev. Lett.* **69**, 2001 (1992); N. Trivedi and M. Randeria, *Phys. Rev. Lett.* **75**, 312 (1995);
- [12] R.R. dos Santos, *Phys. Rev. B* **50**, 635 (1994).
- [13] J.M. Singer, M.H. Pedersen, T. Schneider, H. Beck, and H.-G. Matuttis, *Phys. Rev. B* **54**, 1286 (1996).
- [14] M.H. Pedersen, J.J. Rodríguez-Núñez, H. Beck, T. Schneider, and S. Schafroth, *Z. Phys. B* **103**, 21 (1997).
- [15] M. Letz and R.J. Gooding, *J. Phys.: Condens. Matter* **10**, 6931 (1998).
- [16] M. Keller, W. Metzner, and U. Schollwöck, *Phys. Rev. B* **60**, 3499 (1999).
- [17] J.M. Singer, T. Schneider, and P.F. Meier, in *Symmetry and Pairing in Superconductors*, edited by M. Ausloos and S. Krichinin (Kluwer Academic Publishers, The Netherlands, 1999).
- [18] C.N. Yang, *Phys. Rev. Lett.* **63**, 2144 (1989); C.N. Yang and S. Zhang, *Mod. Phys. Lett. B* **4**, 759 (1990).
- [19] C.N. Yang, *Rev. Mod. Phys.* **34**, 694 (1962).
- [20] G.L. Sewell, *J. Stat. Phys.* **61**, 415 (1995).
- [21] H.T. Nieh, G. Su, and B.M. Zhao, *Phys. Rev. B* **51**, 3760 (1995).
- [22] R.R.P. Singh and R.T. Scalettar, *Phys. Rev. Lett.* **66**, 3203 (1991).
- [23] F.H.L. Eßler, V.E. Korepin, and K. Schoutens, *Phys. Rev. Lett.* **68**, 2960 (1992).
- [24] F.H.L. Eßler, V.E. Korepin, and K. Schoutens, *Phys. Rev. Lett.* **70**, 73 (1993); J. de Boer, V.E. Korepin, and A. Schadschneider, *Phys. Rev. Lett.* **74**, 789 (1995); J. de Boer and A. Schadschneider, *Phys. Rev. Lett.* **75**, 4298 (1995); A. Schadschneider, *Phys. Rev. B* **51**, 10 386 (1995).
- [25] K.A. Penson and M. Kolb, *Phys. Rev. B* **33**, 1663 (1986); *J. Stat. Phys.* **44**, 129 (1986).
- [26] I. Affleck and J.B. Marston, *J. Phys. C: Solid St. Phys.* **21**, 2511 (1988).
- [27] G. Bouzerar and G.I. Japaridze, *Z. Phys. B* **104**, 215 (1997).
- [28] B. Bhattacharyya and G.K. Roy, *J. Phys.: Condens. Matter* **7**, 5537 (1995).
- [29] A.E. Sikkema and I. Affleck, *Phys. Rev. B* **52**, 10 207 (1995).
- [30] J. Hubbard, *Proc. R. Soc. A* **276**, 238 (1963); S. Kivelson, W.-P. Su, J.R. Schrieffer, and A.J. Heeger, *Phys. Rev. Lett.* **58**, 1899 (1987).
- [31] E. Fradkin and J.E. Hirsch, *Phys. Rev. B* **27**, 1680 (1983); K. Miyake, T. Matsuura, H. Jichu, and Y. Nagaoka, *Prog. Theor. Phys.* **72**, 1063 (1983).
- [32] S. Robaszkiewicz, R. Micnas, and J. Ranninger, *Phys. Rev. B* **36**, 180 (1987); C. Bastide and C. Lacroix, *J. Phys. C: Solid St. Phys.* **21**, 3557 (1988).
- [33] A. Hui and S. Doniach, *Phys. Rev. B* **48**, 2063 (1993).

- [34] A. Belkasri and F.D. Buzatu, Phys. Rev. B **53**, 7171 (1996).
- [35] M. van den Bossche and M. Caffarel, Phys. Rev. B **54**, 17 414 (1996).
- [36] G.I. Japaridze and E. Müller-Hartman, J. Phys.: Condens. Matter **9**, 10 509 (1997).
- [37] S. Robaszkiewicz and B.R. Bulka, Phys. Rev. B **59**, 6430 (1999).
- [38] A. Auerbach *Interacting Electrons and Quantum Magnetism*, Springer-Verlag (1994).
- [39] H. Frahm and V.E. Korepin, Phys. Rev. B **52**, 10553 (1990); N. Kawakami and S.-K. Yang, Phys. Lett. A **148**, 359 (1990).
- [40] A. Luther and I. Peschel, Phys. Rev. B **12**, 3908, (1975).
- [41] For a recent review see A.O. Gogolin, A.A. Nersesyan, and A.M. Tsvelik, *Bosonization and strongly correlated systems*, Cambridge University Press (1998).
- [42] P. Wiegmann, J. Phys. C: Solid St. Phys. **11**, 1583 (1978).
- [43] J.M. Kosterlitz and D. Thouless, J. Phys. C: Solid St. Phys. **6**, 1181 (1973).
- [44] K.A. Muttalib and V.J. Emery, Phys. Rev. Lett. **57**, 1370 (1986); T. Giamarchi and H.J. Schulz, Phys. Rev. B **33**, 2066 (1988).